PARTIALLY BLIND DEBLURRING OF BARCODE FROM OUT-OF-FOCUS BLUR

YIFEI LOU, ERNIE ESSER, HONGKAI ZHAO AND JACK XIN*

Abstract. This paper addresses the nonstationary out-of-focus (OOF) blur removal in the application of barcode reconstruction. We propose a partially blind deblurring method when partial knowledge of the clean barcode is available. In particular, we consider an image formation model based on geometrical optics, which involves the point-spread function (PSF) for the OOF blur. With the known information, we can estimate a low-dimensional representation of the PSF using the Levenberg-Marquardt algorithm. Once the PSF is obtained, the image deblurring is followed by quadratic programming. We find [0,1] box constraint is often good enough to enforce binary signal. Experiments on the real data demonstrate that the forward model is physically realistic and our partially blind deblurring method can yield good reconstructions.

Key words. barcode, out-of-focus blur, geometrical optics, Levenberg-Marquardt algorithm, quadratic programming, box constraint

AMS subject classifications.
90C90, 65K10, 49N45, 49M20, 78A05

1. Introduction . Image restoration from out-of-focus (OOF) blur is a very difficult problem, as one has to infer both the original image and the point-spread function (PSF) from the data. Most conventional methods model the OOF blur as a uniform disk [29, 25] and hence the PSF estimation reduces to estimating the radius of the blur disk [27]. However, in the real scenario, the OOF blur is not uniform, but dependent on the geometry of the object. The nonstationary nature makes many blind deconvolution methods [7, 2, 24] unapplicable for the OOF blur removal. One way to manage spatially variant blur is to segment the data into regions, on each of which blur is approximately invariant. This idea has been explored in [28, 21, 8, 5]. However, deblurring results suffer from ringing artifacts due to the inconsistency of boundaries between different regions. A related line of research in modeling the OOF blur is the shape from defocus [14, 16]. Although the main focus is to reconstruct the 3D geometry of a scene from a set of defocused images, image deblurring can be a byproduct. However, this type of approach often requires a well-calibrated camera and multiple images as input, which limits their usage in image deblurring from the OOF blur.

We attempt to solve this OOF deblurring problem in the application of barcode reconstruction. Standard commercial techniques are based on classic edge detection [22, 23]. Since edges are important for barcode decoding, one searches for local extrema of the derivative of the signal, which hopefully correspond to edges. However, this approach has two main drawbacks. First of all, the derivative is highly sensitive to small changes in the data, such as noise. In addition, some edges in the original barcode may not have corresponding extrema in the corrupted data if the blur is relatively large. An alternative direction of barcode decoding is to view it as a deblurring problem. Most of works assume that the PSF is a shift-invariant kernel and then blind or nonblind deconvolution is formulated to reconstruct the barcode. For example, variational models are discussed in [12, 9]. Recently, Iwen *et. al.* [20] develop a sparse representation of the barcode by exploiting the barcode symbology. These methods are not exactly blind, but can deal with small amount of blurring and noise.

We propose a partially blind method to recover binary barcode. It is based on an image formation model for out-of-focus blur [15]. We first estimate a low-dimensional approximation to the PSF by using some parts of clean barcode that are known by construction. This low-dim representation only involves a few parameters, which can be iteratively computed via the Levenberg-Marquardt (LM) algorithm. The rest of the PSF is obtained by polynomial interpolations. Next, image deblurring is performed by solving the least-square (LS) solution with additional constraint that the variables are bounded by 0 and 1, *i.e.* $[0, 1]$ box constraint. We further take the minimum bar width into account, which corresponds to a stretching matrix or an up-sampling operator. Having this matrix in the LS

* All authors are from Department of Mathematics, UC Irvine, Irvine, CA 92697. Emails: ylou1@uci.edu, eesser@uci.edu, zhao@math.uci.edu, jxin@math.uci.edu.

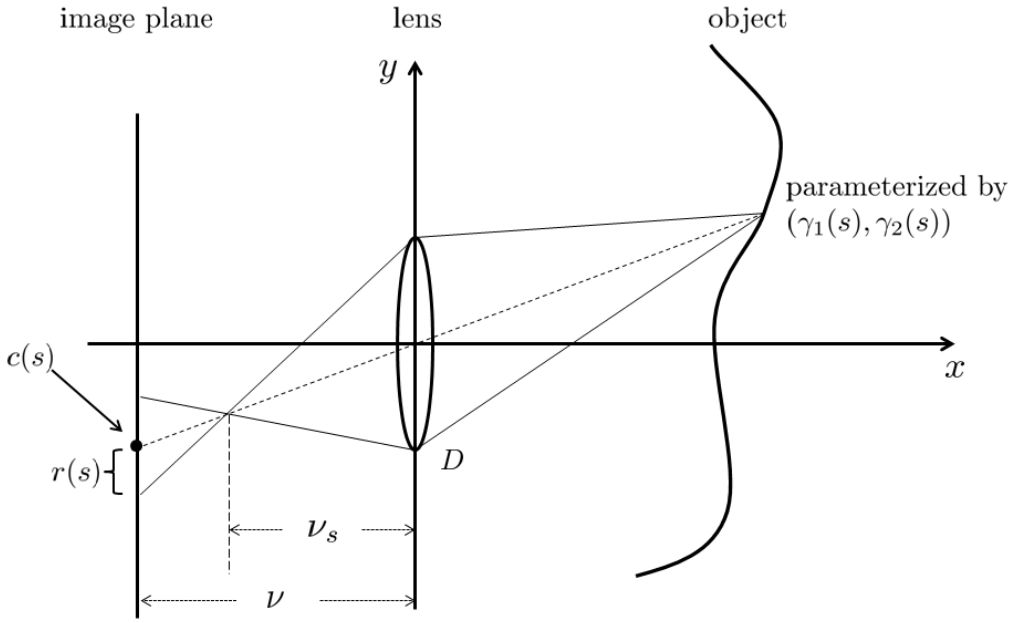

FIG. 2.1. *The geometry of an imaging system. The camera is represented by an image plane and a lens. The image plane is placed at the distance ν to the lens. The lens has diameter/aperature D and focal length F. The depth map of an object is parameterized by its arc length: $s \mapsto: (\gamma_1(s), \gamma_2(s))$. Any point source of s on the object produces a blur spot on the image plane that is centered at $c(s)$ with radius $r(s)$. The thin lens formula [19] is satisfied for $\gamma_1(s)$, ν_s and F. Please refer to Appendix for more details.*

term largely enhances the efficiency of image deblurring. In summary, our contributions are three-fold.

1. We consider an image formation model for out-of-focus blur based on geometrical optics. In Section 4.1, we demonstrate it is a physically realistic model by matching the real data with the synthetic ones.
2. Using barcode's known information, we adopt the Levenberg-Marquardt algorithm to estimate a low-dimensional representation of the PSF .
3. Once the PSF is obtained, a deblurred signal can be obtained by simple quadratic programming: least-square solution with $[0, 1]$ box constraint. We notice that in most cases box constraint is good enough to enforce binary signal.

The rest of the paper is organized as follows. Section 2 describes our problem settings including an image formation model and the barcode representation. Section 3 details our partially blind deblurring algorithm. Numerical experiments are presented in Section 4 where both real and synthetic data are examined. Section 5 is devoted to an extension to 2D Quick Response (QR) barcodes. Finally, conclusions and future work are given in Section 6.

2. Problem Settings.

2.1. Basic Image formation model. We consider an image formation model for out-of-focus blur based on geometrical optics. Assume that a schematic camera is composed of an image plane and a lens, as depicted in Figure 2.1. The image plane contains a number of CCD[1] sensors that

[1]CCD: charge-coupled device.

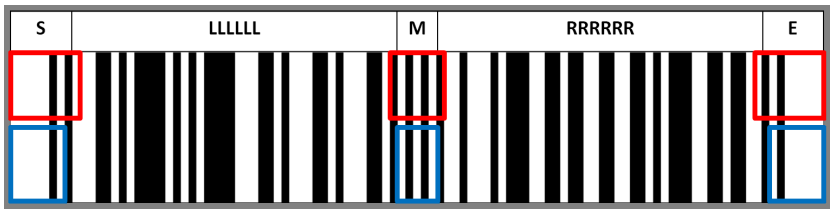

FIG. 2.2. *Barcode's symbology. Each barcode follows the pattern SLLLLLLMRRRRRRE, where the S (start), M (middle), and E (end) guard bars are fixed for every barcode and the L (left) and R (right) sections collectively represent the 12 numerical digits. The top large rectangles in red indicate where the barcode information is known, while the bottom ones in blue are the regions where the data is unaffected by the unknown pixels. We use the data in blue regions together with the known information of the clean barcode to estimate the PSF. Ideally the size of the blue regions should be adjusted according to how severe the blur is. As there is no automatic way of doing it, we fix these regions through experiments.*

record the amount of light received at a particular location. The lens is a device that alters light propagation via diffraction. For a thin (approximately planar) circular lens, it is shown in [1] that a point of light emitting from the source produces a blur spot on the image plane, known as *circle of confusion*. Suppose the light source comes from an object with depth map parameterized by its arc length $s \in \Omega \mapsto (\gamma_1(s), \gamma_2(s))$. Any point source of s emits light with infinitesimal intensity $u(s)\mathrm{d}s$, where $u(s)$ is the radiance function of the object. The weighted combination of the contributions from all points forms an image on the image plane, denoted as $f(y)$. The weight, often referred to as the point-spread function, is assumed to be a Gaussian function, which is centered at $c(s)$ with standard deviation being the radius of the disk $r(s)$. To summarize, our image formation model can be expressed as follows,

$$f(y) = \int_{s\in\Omega} \frac{1}{\sqrt{2\pi}r(s)} \exp^{-\frac{(y-c(s))^2}{2r^2(s)}} u(s)\mathrm{d}s \ . \tag{2.1}$$

Both $c(s)$ and $r(s)$ are derived from the object's depth map $(\gamma_1(s), \gamma_2(s))$. Please refer to Appendix for more details. Note that the PSF is not a shift-invariant kernel and thus there is no fast implementation via convolution and fast Fourier transform. Only when the object is parallel to the lens, *i.e.*, $\gamma_1(s)$ is constant, this model (2.1) becomes the classical shift-invariant blur.

Note that eq. (2.1) is a pure mathematical abstraction, as the thin circular lens is the idealized model and light propagation phenomena are subject to a variety of effects. Simplified though, it is a realistic model. As demonstrated in Section 4.1, we use this model to artificially blur the barcode signal, which matches with the real image we capture from a commercial camera.

2.2. Barcode representation. A one-dimensional barcode is a finite series of alternating black bars and white spaces whose relative widths encode information. The most common is probably the UPC-A barcode used in supermarkets. In the UPC-A symbology, each barcode consists of 12 numerical digits. As present in Figure 2.2, a typical UPC-A barcode follows the pattern SLLLLLLMRRRRRRE, where the S (start), M (middle), and E (end) guard bars are represented exactly the same for every barcode and the L (left) and R (right) sections collectively represent the 12 numerical digits that make each barcode unique.

In the sequel, we represent a white bar of unit width by 0 and black bar by 1[2]. The patterns for S, M, E are S=E=101 and M=01010 respectively. Each digit is represented by 7 modules. For example, the left-hand "6" digit is represented by the sequence 0101111; its right-hand version is 1010000. Accordingly, a barcode can be represented by a 95-dim binary vector $\mathbf{x}$ with the $7 \times 12 = 84$ modules for the digits (L and R) and 11 modules for S, M, and E patterns.

[2]Note that it is unconventional color coding; usually white is mapped to 1, and black to 0.

Given the blurred data f in (2.1), we exploit the known information of a barcode to estimate the PSF. For example, the patterns on the S, M, E regions are fixed for any barcode. In order to better utilize the information on S and E regions, we elongate the binary vector $\mathbf{x}$ by zero padding on both sides. This is reasonable, as the barcode is always surrounded by the white areas. More importantly, it contains useful information to understand how the boundary gets blurred. We further notice that the first and the last elements for each digit, no matter whether it appears in L or in R, are always the same. We will use these regions, as indicated in red rectangles in Figure 2.2, where barcode information is known to estimate the PSF.

3. Algorithm. We propose a "partially" blind restoration method in the sense that we exploit the known barcode information to estimate the PSF. Then image deblurring is performed using the estimated PSF with additional constraint that the signal is binary.

3.1. Estimating the PSF. We compute the PSF based on obtained data and the known information of the barcode. For the out-of-focus blur, the PSF is characterized by the center and the blur radius of each point source, $c(s)$ and $r(s)$. We consider a low-dimensional representation by polynomial interpolation . In particular, we approximate $c(s)$ using 6 data points (two in each known region: S, M and E), denoted as s_j for $j = 1, \cdots, 6$. Given values of $c(s)$ at these 6 points, we can define a matrix P with each row being $P_j = [s_j^3 \ s_j^2 \ s_j \ 1]$. Denote $\hat{c}(s)$ as a third-order polynomial to approximate $c(s)$:

$$\hat{c}(s) = c_3 s^3 + c_2 s^2 + c_1 s + c_0 \ . \tag{3.1}$$

The coefficients of $\hat{c}(s)$ can be calculated by a least-square fitting, *i.e.*,

$$\begin{bmatrix} c_3 \\ c_2 \\ c_1 \\ c_0 \end{bmatrix} = (P^T P)^{-1} P^T \begin{bmatrix} c(s_1) \\ \vdots \\ c(s_6) \end{bmatrix} \ . \tag{3.2}$$

Similarly we can obtain the polynomial $\hat{r}(s)$ to approximate $r(s)$. The polynomial approximation is reasonable, considering that the depth map is continuous and so are $c(s)$ and $r(s)$. With polynomial interpolations, the PSF is now dependent on 12 parameters $\boldsymbol{\theta} = [c(s_j), r(s_j)]_{j=1,\cdots,6}$, which is a large dimension reduction.

In order to estimate $\boldsymbol{\theta}$, we modify the image formation model (2.1) so that it explicitly depends on $\boldsymbol{\theta} = \{\theta_k\}_{k=1,\cdots,12}$ and the known information of the barcode. Denote R as the region where the barcode information is known. The discrete version of (2.1) is

$$\hat{f}(y;\boldsymbol{\theta}) = \sum_{s\in R} \frac{1}{\sqrt{2\pi}\hat{r}(s)} \exp^{-\frac{(y-\hat{c}(s))^2}{2\hat{r}^2(s)}} u(s), \tag{3.3}$$
for $\hat{c}(s), \hat{r}(s)$ being interpolated from $\boldsymbol{\theta}$.

We further restrict the domain of the data points by considering $y \in B$ where the data is unaffected by the unknown barcode. Notice that ideally we should adjust the data region B according to how severe the blur is. But as there is no automatic way of doing it, we fix the size of B through experiments. In Figure 2.2, the red triangles indicate the known barcode regions R, while the blue ones are the regions B for the data points we use to estimate the PSF.

Given the known barcode signal $x \in R$ and the data points $y \in B$, we adopt the Levenberg−Marquardt (LM) scheme to find $\boldsymbol{\theta}$ that minimizes

$$S(\boldsymbol{\theta}) = \sum_{y\in B} \|f(y) - \hat{f}(y;\boldsymbol{\theta})\|^2. \tag{3.4}$$

Since $S(\boldsymbol{\theta})$ is nonlinear and implicit with respect to $\boldsymbol{\theta}$, the Jacobian is computed numerically for each component of $\boldsymbol{\theta}$,

$$J_k = \frac{1}{\epsilon}\left(\hat{f}(y;\boldsymbol{\theta} + \epsilon \mathbf{1}_k) - \hat{f}(y;\boldsymbol{\theta})\right) \ , \tag{3.5}$$

where $\mathbf{1}_k$ is an indicator vector with 1 at the index k. At every iteration, the increment $\boldsymbol{\delta}$ is solved from the linear system,

$$(J^T J + \lambda \boldsymbol{I})\boldsymbol{\delta} = J^T[f(y) - \hat{f}(y;\boldsymbol{\theta})] \ . \tag{3.6}$$

The parameter $\lambda \geqslant 0$ is adjusted at each iteration. If reduction of S is sufficient, a smaller value is used; whereas if an iteration gives insufficient reduction in the residual, we should increase its value. Once the values $\boldsymbol{\theta}$ are obtained, we can compute $\hat{c}(s)$ and $\hat{r}(s)$ as approximations to $c(s)$ and $r(s)$ and accordingly the PSF can be calculated via eq. (2.1).

Note that a fast alternative is to use a piece-wise convolution approximation to the full blurring model. However, experiments indicate that it is more prone to getting stuck in local minima, partly because fewer equations are used in order to avoid boundary artifacts.

3.2. Image deblurring. The discrete imaging model (2.1) can be expressed as matrix-vector multiplication $\mathbf{f} = H\mathbf{u}$. The blurring matrix H is estimated via the LM algorithm, as detailed in the previous section.

We take into account the minimum bar width to reduce the computational cost. Suppose the barcode signal $\mathbf{x} = [x_1, \cdots, x_n]$ is of length n after zero padding. Consider the characteristic function

$$\chi(t) = \begin{cases} 1 & \text{for } 0 \leqslant t \leqslant 1, \\ 0 & \text{else.} \end{cases}$$

Then the barcode function can be further represented as

$$u(s) = \sum_{j=1}^{n} x_j \chi(\frac{s}{w} - j) \tag{3.7}$$

where w is the minimum bar width. In the discrete version, this is equivalent to $\mathbf{u} = \mathcal{S}\mathbf{x}$ with $\mathcal{S}$ being a stretch matrix. It can be defined in terms of the Kronecker product, *i.e.*, $\mathcal{S} = I_n \otimes 1_w$, where I_n is an identity matrix of size n and 1_w is a column vector of length w with element 1. It is huge dimension reduction to solve $\mathbf{x}$ instead of $\mathbf{u}$.

Let $A = H\mathcal{S}$. We formulate the image deblurring problem as a least-square fitting with binary constraint,

$$\min \|A\mathbf{x} - \mathbf{f}\|^2 \qquad \text{s.t.} \quad \mathbf{x} \in \{0, 1\} \tag{3.8}$$

This is a non-convex problem due to the binary constraint. There are a couple of natural strategies for solving the original problem (3.8). One is to relax the binary constraint by box constraint (BX),

$$\min \|A\mathbf{x} - \mathbf{f}\|^2 \qquad \text{s.t.} \quad 0 \leqslant \mathbf{x} \leqslant 1 \tag{3.9}$$

This is a quadratic programming problem, which is well-studied and can be solved by many optimization schemes. We adopt a modified primal dual hybrid gradient (PDHG) method [30] to solve it. The PDHG method [30] and its variants [4, 13, 18] can be used to solve general convex optimization problems of the form

$$\min_{\mathbf{x}} J(A\mathbf{x}) + H(\mathbf{x})$$

where J and H are closed proper convex functions. They find a minimizer $\mathbf{x}^*$ by solving for a saddle point $(\mathbf{x}^*, \mathbf{y}^*)$ of

$$L(\mathbf{x}, \mathbf{y}) = H(\mathbf{x}) + \langle \mathbf{y}, A\mathbf{x} \rangle - J^*(\mathbf{y}) \ .$$

A common variant of PDHG does this by iterating

$$\begin{aligned} \mathbf{y}^{k+1} &= \arg\min_{\mathbf{y}} J^*(\mathbf{y}) - \langle A\mathbf{x}^k, \mathbf{y} \rangle + \frac{1}{2\delta}\|\mathbf{y} - \mathbf{y}^k\|^2 \\ \mathbf{x}^{k+1} &= \arg\min_{\mathbf{x}} H(\mathbf{x}) + \langle A^T(2\mathbf{y}^{k+1} - \mathbf{y}^k), \mathbf{x} \rangle + \frac{1}{2\alpha}\|\mathbf{x} - \mathbf{x}^k\|^2 \ , \end{aligned}$$

where δ and α are positive parameters satisfying $\alpha\delta < \frac{1}{\|A^TA\|}$ and J^* denotes the Legendre transform or convex conjugate of J. This method is especially useful when the J and H minimization subproblems can be efficiently solved. Moreover, it is not necessary to explicitly construct the matrix A since the method only requires that we be able to multiply by A and A^T. For Problem (3.9), we let $J(A\mathbf{x}) = \frac{1}{2}\|A\mathbf{x}-\mathbf{f}\|^2$ and $H(\mathbf{x}) = g_{[0,1]}(\mathbf{x})$, where g is an indicator function defined by $g(x) = \begin{cases} 0 & \text{if } x \in [0,1] \\ \infty & \text{otherwise.} \end{cases}$ Since $J^*(\mathbf{y}) = \frac{1}{2}\|\mathbf{y}\|^2 + \langle f, \mathbf{y}\rangle$, the explicit iterations can be written in closed form as

$$\mathbf{y}^{k+1} = (\delta A\mathbf{x}^k - \delta\mathbf{f} + \mathbf{y}^k)/(1+\delta) \tag{3.10}$$

$$\mathbf{x}^{k+1} = \Pi_{[0,1]}\big(\mathbf{x}^k - \alpha A^T(2\mathbf{y}^{k+1} - \mathbf{y}^k)\big) \tag{3.11}$$

where $\Pi_{[0,1]}$ denotes the orthogonal projection onto $[0,1]$. For this application, the method is closely related to simple gradient projection, *i.e.* equivalent if $\delta = 1$. There are accelerated variants to improve the rate of convergence.

Another way is to enforce the binary constraint by using the double well (DW) potential [12]

$$\mathbf{x} = \arg\min \frac{1}{\epsilon}W(\mathbf{x}) + \epsilon\|D\mathbf{x}\|^2 + \frac{\gamma}{2}\|A\mathbf{x}-\mathbf{f}\|^2 \tag{3.12}$$

where $W(x) = x^2(1-x)^2$ and ϵ, γ are two positive parameters. Including the derivative term $\|D\mathbf{x}\|$ helps to suppress the spatial oscillations. Both DW without $\|D\mathbf{x}\|$ and the box constraint (3.9) suffer from this artifact. We apply gradient descent to obtain the optimal solution:

$$\mathbf{x}_t = -\frac{1}{\epsilon}W'(\mathbf{x}) + \triangle\mathbf{x} - \gamma A^T(A\mathbf{x}-\mathbf{f}) \ . \tag{3.13}$$

4. Numerical Experiments. We validate the image formation model (2.1) by matching the real data with the synthetic ones. Deblurring results are present for both real data and synthetic ones. We also examine the performance of some components of our algorithm using synthetic data. Our Matlab source codes are available for download at the project webpage: `https://sites.google.com/site/louyifei/research/barcode`.

4.1. Model validation. We demonstrate the image formation model (2.1) is realistic by matching real signals with synthesized data. We take real images of barcodes. The top left plot in Figure 4.1 is an image of Huggies diaper barcode printed on a box taken by Iphone5 and the more blurred one on the right is of Kirkland's plastic wrap barcode taken by Canon SLR Rebel XTi camera. Each row of the image (except for the lower part with numbers) can be regarded as 1D corrupted barcode. The real data to be processed, denoted as f, is the average of a number of rows for the purpose of eliminating noises. We manually adjust the intensity value so that the synthetic data fit better with the real ones. An automatic way of intensity fitting is addressed in Section 4.2. The intensity transforms are $1.2 - 1.6f$ and $1 - 1.38f$ for diaper box and wrap case respectively. The negative sign is due to barcode's unconventional color coding that maps white to 0 and black to 1.

To compare the real data with the synthetic ones, we first estimate the bar width from the data f. We detect its local minima, each ideally corresponding to the center of black bar. Using the fact that the barcode is a 95-dim binary vector, we set the bar width to be the number of pixels between the first and the last minimum locations divided by 94. The division by 94 instead of 95 is because that half bars on two ends are not counted in the range of two minima. The bar width of the diaper box is calculated as 18.6, and we round it off to 19. The bar width for the wrap case is 8.

We synthesize blurred data from the model (2.1) in the following way. We generate a ground-truth barcode using 12-number digits present in the image. For diaper box, we pad its 95-dim vector with six '0's on two sides and stretch it by a factor of 19. Similarly for the wrap case except that the stretch factor is 8. We fix the camera parameters to be: focal length $F = 12e-3$, distance between image plane and the lens $\nu = 0.01285$. Since the depth map is a linear function for both diaper box and wrap

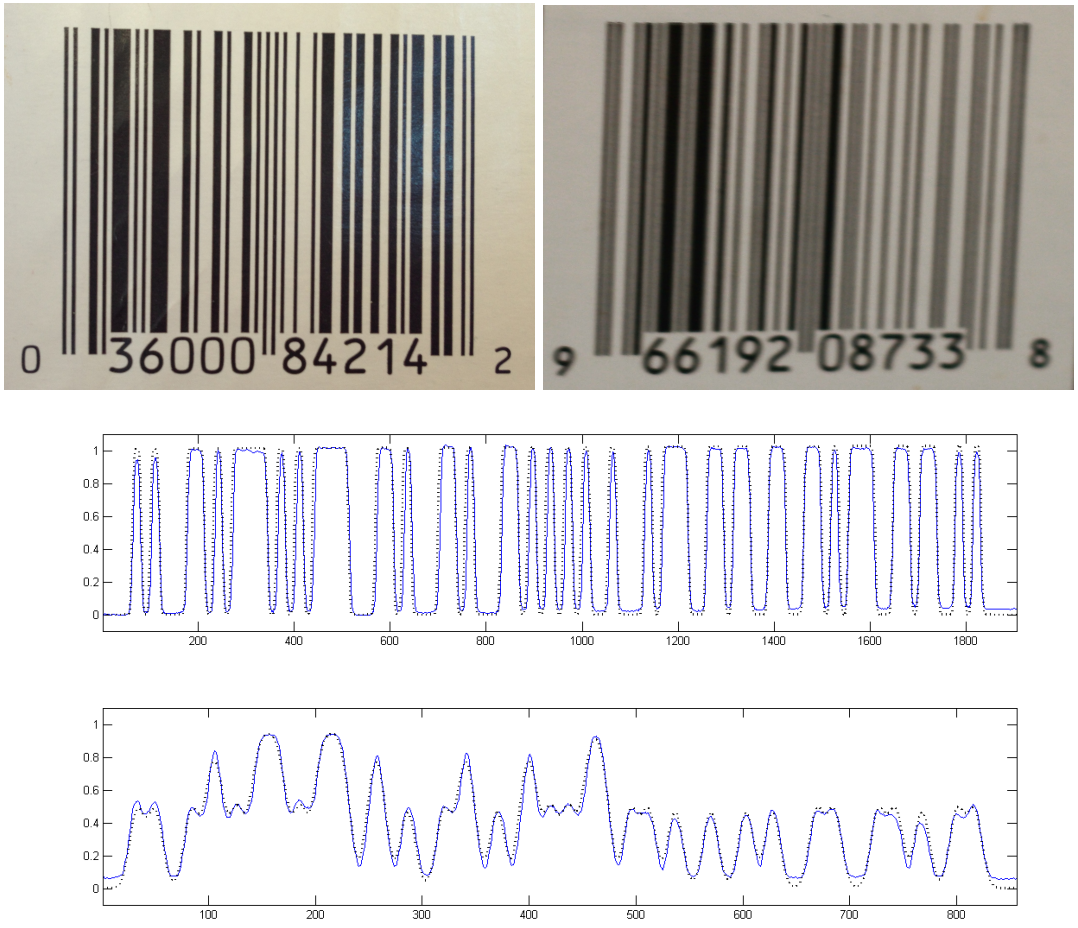

FIG. 4.1. *Model validation by fitting the real data with the synthetic ones. Two real images are displayed: top left is barcode on a diaper box, and top right is on a plastic wrap case. The real 1D data to be processed is the average of several rows of the image for the purpose of eliminating noises. The last two rows illustrate that the synthetic data (in black dotted line) using the generative model (2.1) fit nicely with the real data (in blue).*

case, we manually tune parameters a, b to match the synthetic blurred data with real ones. We find $a = 0.01, b = 1.015$ and aperture $D = 0.0472$ for diaper box and $a = 0.02, b = -0.95, D = 0.2629$ for wrap box give good matches, as shown in Figure 4.1. This demonstrates that the generative model (2.1) we use throughout the paper is realistic.

In what follows, we examine the performance of some components of our algorithm using synesthetic data. The ground-truth signal is the barcode of the diaper box, zero-padding is of size 4 on each side and the stretch factor is 19.

Polynomial interpolation. More often than not, the barcode appears on a planar surface. As a result, both $c(s)$ and $r(s)$ are rational functions according to eq. (6.2) in the Appendix. We discuss the interpolation errors using third-order polynomials.

We vary the slope of the plane a from -0.2 to 0.2 and intercept b from 0.8 to 1.2 with increment 0.02. For each combination, we generate the ground-truth center function $c(s)$ and radius function $r(s)$ using eq. (6.2). Given the exact values of $c(s)$ and $r(s)$ at 6 key points $s_j, j = 1, \cdots, 6$, we can obtain their interpolated versions $\hat{c}(s), \hat{r}(s)$ by eq. (3.1). We plot the errors in terms of $\|c - \hat{c}\|_2$ and $\|r - \hat{r}\|_2$ in Figure 4.2. The approximation errors are in order of $o(1)$ and $o(10^{-6})$ for $c(s)$ and $r(s)$ respectively. This demonstrates that it is reasonable to approximate $c(s)$ and $r(s)$ by low-dimensional

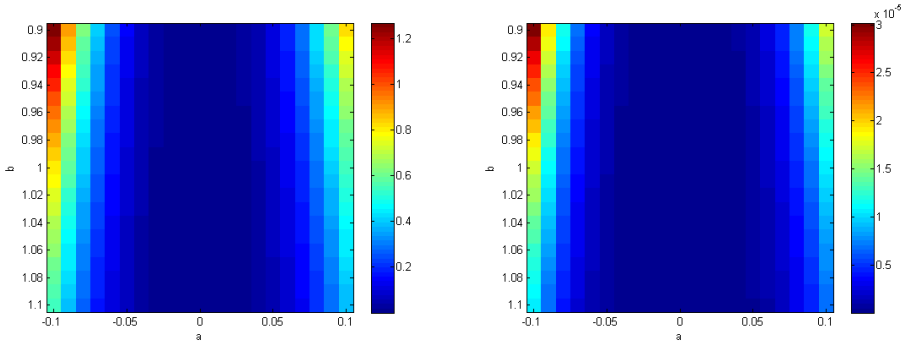

FIG. 4.2. *Interpolation errors of $c(s)$ and $r(s)$ using third-order polynomials for different combinations of slope a and intercept b.*

	$a = 0.01,\ b = 1.01$		$a = -0.01,\ b = 0.995$		$a = 0.02,\ b = 1.02$	
	$c(s) - \hat{c}(s)$	$r(s) - \hat{r}(s)$	$c(s) - \hat{c}(s)$	$r(s) - \hat{r}(s)$	$c(s) - \hat{c}(s)$	$r(s) - \hat{r}(s)$
s_1	-0.0009	-0.0055	-0.00107	-0.0081	0.0268	-0.6798
s_2	0.0010	0.0062	0.0008	0.0092	0.0397	0.0647
s_3	0.0013	-0.0010	-0.0004	-0.0007	0.0393	0.0080
s_4	-0.0016	-0.0004	0.0001	-0.00014	-0.0014	-0.0157
s_5	0.0017	0.0058	0.0009	0.0090	-3.1857	20.0433
s_6	-0.0015	-0.0051	-0.0008	-0.0080	-3.6019	23.4362

TABLE 4.1
Point-wise difference of $c(s) - \hat{c}(s)$ and $r(s) - \hat{r}(s)$ at $s_j, j = 1, \cdots, 6$ for three combinations of a, b.

polynomials.

The PSF estimation. We examine the performance of the PSF estimation using LM. In Table 4.1, we record the point-wise difference of $c(s) - \hat{c}(s)$ and $r(s) - \hat{r}(s)$ at $s_j, j = 1, \cdots, 6$ for three combinations of a, b. The last example in Table 4.1, when $a = 0.02, b = 1.02$, reveals the limitation of our method. When a, b are further away from 0 and 1, there are larger shifts present in the data, especially in the known barcode regions S and E. If we choose the region B to be large, (*i.e.* more data points are used), then some of the data points are affected by the unknown barcode. If a smaller size of B is used, then we do not have enough equations to estimate the PSF. In order to get a good estimation of the PSF, there are empirical bounds of a, b, which are roughly $a \in [-0.01, 0.01]$ and $b \in [0.99, 1.01]$.

We compare the full blurring model (3.3) with a piece-wise convolution approximation. The data model is:

$$S(\boldsymbol{\tau}_i) = X(k(\boldsymbol{\tau}_i) * u_i - f_i) \tag{4.1}$$

where i indexes the reference location, X is a cropping matrix, u_i is an interval from the reference barcode, f_i is the roughly corresponding interval from the blurry barcode, and $\boldsymbol{\tau}_i$ is a length 2 vector of the shift and blur parameters at each location. The LM method is used to minimize

$$||S(\boldsymbol{\tau})||^2 + v||R\boldsymbol{\tau}||^2,$$

where the regularizer R encourages $\boldsymbol{\tau}$ to be close to a smooth curve that approximately interpolates $\boldsymbol{\tau}$, *i.e.*, trying to balance between data fitting and minimizing curvature. Because the setup is different from the full model (3.3), we can not compare them in terms of poise-wise errors as in Table 4.1. Instead, we list the estimation errors of the blurring matrix in Table 4.2. It shows that full model yields significantly smaller errors compared to the piece-wise convolution approximation. This may

	$a = 0.01,\ b = 1.01$	$a = -0.01,\ b = 0.995$	$a = 0.02,\ b = 1.02$
full model (3.3)	$9.97e^{-5}$	$1.18e^{-4}$	9.69
piece-wise convolution (4.1)	16.43	8.36	19.95

TABLE 4.2

Comparison to a piece-wise convolution model to estimate the PSF for three combinations of a, b. The errors are measured by the Frobenius norm of difference between the ground-truth blurring matrix H and the estimation using full model or piece-wise convolution.

noise std	$c(s)$	$r(s)$	DW without $\mathcal{S}$	BX without $\mathcal{S}$	DW with $\mathcal{S}$	BX with $\mathcal{S}$
0	2.84	0.44	0	0	0	0
0.05	9.98	26.23	0.32	0.77	0	0
0.1	19.38	51.02	1.08	2.20	0	0
0.25	75.13	194.71	4.62	9.72	1.07	0.58
0.5	367.25	677.91	19.38	22.34	12.04	12.52

TABLE 4.3

Errors under different noise levels. Each reported value is the mean of 10 random realizations. The errors of $c(s)$ and $r(s)$ are measured by the L^2 norm, while the ones of DW and BX are measured by the ratio of the L^1 difference norm to the length of the signal in %.

be because fewer equations are used in order to avoid boundary artifacts and parameters at different locations are less strongly coupled. On the other hand, the piece-wise convolution model (4.1) is much faster than the full model, that is, seconds instead of minutes. It works well for small displacements.

Deblurring performance with noise We investigate the robustness of our algorithm with respect to noise. We use the synthetic data that matches with the real data of the diaper box; in other words, we choose $a = 0.01, b = 1.015$. We randomly add white Gaussian noise to the data with different standard deviations. Table 4.3 lists the L^2 norm of $\|\hat{c}(s) - c(s)\|$ and $\|\hat{r}(s) - r(s)\|$, and the reconstruction errors measured by the ratio of the L^1 difference norm between the estimated signal and the original one to the length of the signal. Each reported value is the mean of 10 random realizations. Although large errors occur in estimating $c(s)$ and $r(s)$, DW and BX are still able to reconstruct the barcode signal with the stretching matrix. Without this matrix, DW is less susceptible to noise compared with BX, because the box constraint is no longer a good relaxation to the binary constraint in the presence of large noise.

Box constraint. The original deblurring problem (3.8) is non-convex. People have noticed that its global minimizer can often be obtained by solving the relaxed convex problem [6, 26]. Although the box constraint does not explicitly enforce binary signal, the solution is almost binary. Figure 4.3 plots the histogram of the LS solutions with and without the stretch matrix, both of which have two spikes at 0 and 1.

We further study the box constraint by deblurring with ground-truth PSF. The errors, measured by the L^1 difference between the solution of (3.9) and the ground-truth, are plotted in Figure 4.4 with varying a and b. Depending on blur, the box constraint can give perfect reconstructions.

Our conjecture is that the LS solution with box constraint (3.9) is consistent with a binary solution if the blurring matrix and the underlying signal satisfy certain conditions. Mao [26] proves that if H is the selection of Fourier coefficients and certain number of low frequency coefficients are known, then the binary solution is the unique LS solution with box constraint. As H is a more general matrix in our case, we can not apply his analysis. For a general matrix, the exact l_1 recovery of sparse solution is studied in [11], in which the uniqueness condition depends on the coherence of the matrix. We plot the histogram of cosine angles of two different column vectors. Two matrices are examined in Figure 4.5: one gives the unique binary solution if box constraint is enforced, and the other does not. We find two histograms look similar, which suggests coherence is probably irrelevant to the equivalence between box and binary constraint. In another related work [3], the authors prove that a sparse nonnegative solution can be uniquely reconstructed as quadratic programming problem. This can be regarded as

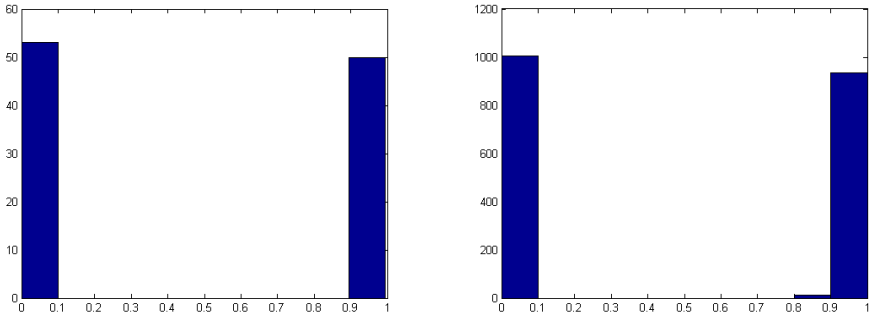

FIG. 4.3. *The histogram of the L-S solution subject to box constraint with (left) or without (right) the stretching matrix.*

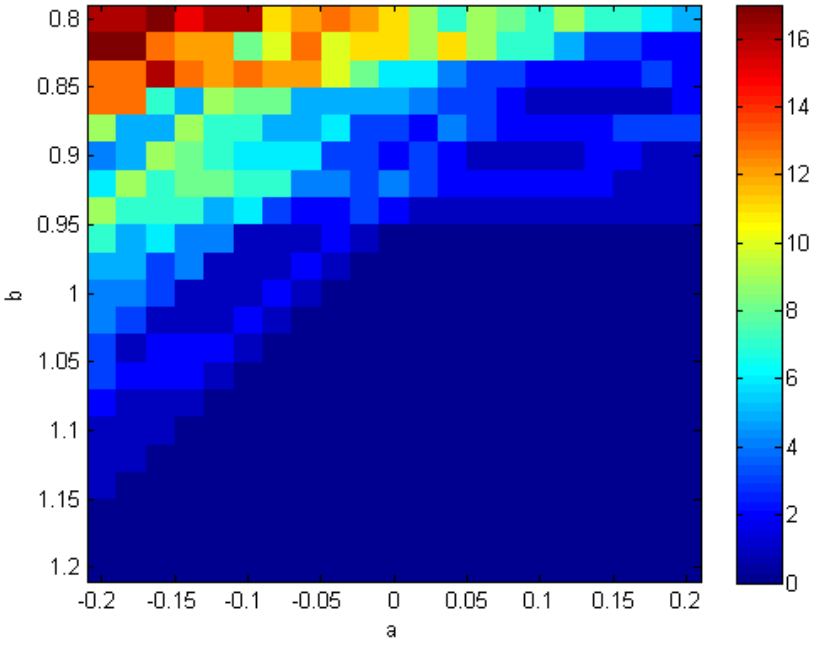

FIG. 4.4. *Errors, measured by the L^1 difference between the solution of (3.9) and the ground-truth, are plotted with varying a, b. In most cases, the box constraint results in perfect reconstructions.*

half of the story in our case with just the nonnegativity, as we also require the upper bound less than 1. The question when the box constraint is equivalent to binary constraint remains open for further investigation.

4.2. Deblurring of real data. In addition to the PSF estimation and image deblurring, as discussed in Section 3, we perform the following pre-processing steps to deal with real images of barcodes: 1) take the average of several rows in the image to suppress the noise; 2) estimate the bar width w = the number of pixels between the first and the last minimum locations divided by 94; 3) the data for deblurring is the central part of length nw with $n = 95$+zero-padding; and 4) To compensate for the illumination changes, the intensity values of real data should be adjusted. We consider a linear transform that maps the smallest intensity value to 1, and largest to 0. However, the smallest/largest

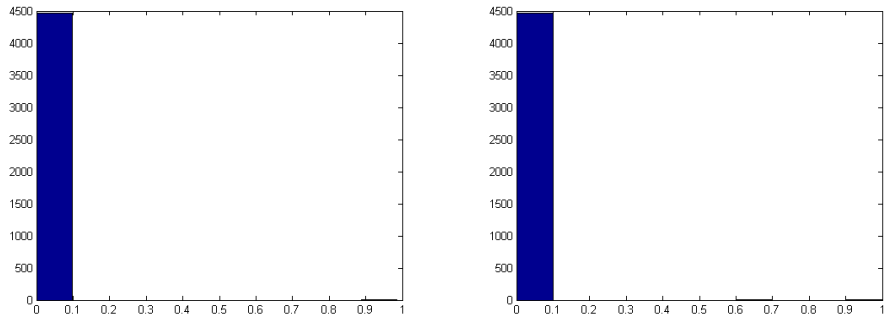

FIG. 4.5. *The histogram of cosine angles of two different column vectors. On the left is of the matrix that yields the unique binary solution if box constraint is enforced, while the other that does not have such property is shown on the right. The maximum value for two histograms are 0.9857 and 0.9989.*

value is very sensitive to noise. Instead, we choose them to be the median of intensities at the first/last peak of histogram bins.

The deblurring results for diaper barcode are illustrated in Figure 4.6. Simple thresholding is used as the initial guess for both BX and DW. Because of the non-uniform shifts in the data, thresholding yields lots of errors, 30%. The stretch matrix plays an important role in both computational efficiency and accuracy. Without this matrix, the reconstructions using either BX or DW still contain 3% of errors, while we can have perfect reconstructions if we take it into account.

It is challenge to deblur the real data of plastic-wrap barcode, as it looks very blurred. With human eyes, one is hard to recognize the middle three bars in the real data, shown on the top of Figure 4.7. The reconstruction of BX with stretching matrix is incorrect for only one bar. DW does not perform very well in this case. This is because that with stretching matrix, each bar is of unit size, which could be smeared out by DW.

4.3. A synthetic example of barcode on a curved surface. The real data present here are images of barcode on the planar surface. With the generative model (2.1), our method should work on any smooth surface. However, we find our algorithm does not work on the real barcode image on a juice bottle. We believe the problem lies in nonlinear interactions of the light reflected on the surface. Our model is only aimed at the geometry of the scene, while not modeling photometrical effects. We will explore with real data on any (curved) surface in the future. Here we present a synthetic example as a proof of the concept. The depth map is chosen to be part of a circle shown on the top of Figure 4.8. Accordingly the center and radius functions, $c(s)$ and $r(s)$ are plotted as well in Figure 4.8. Again our algorithm can give the perfect reconstruction.

5. An extension to two-dimensional QR code restoration. We extend this partially blind deblurring method into 2D. A good example of a 2D barcode is Quick Response (QR) code. A typical QR code is depicted on the top left of Figure 5.1 where three regions as indicated by the red squares are known and the ones in blue are used to estimate the PSF.

Similar to eq. (2.1), the image formation model goes as follows,

$$f(y_1, y_2) = \iint \frac{1}{2\pi r^2(s_1, s_2)} \exp^{-\dfrac{(y_1 - c_1(s_1, s_2))^2 + (y_2 - c_2(s_1, s_2))^2}{2r^2(s_1, s_2)}} u(s_1, s_2) \mathrm{d}s_1 \mathrm{d}s_2 \ . \tag{5.1}$$

In the 2D case, there are three functions, $c_1(s_1, s_2), c_2(s_1, s_2), r(s_1, s_2)$, to be estimated. We choose 4 points in each known region (12 in total), to approximate these functions by 2D polynomials. Once the PSF is obtained, the difficulty lies in the image deblurring as the blurring matrix H is too large to store. For both box constraint and double-well potential, the algorithm only involves the computation

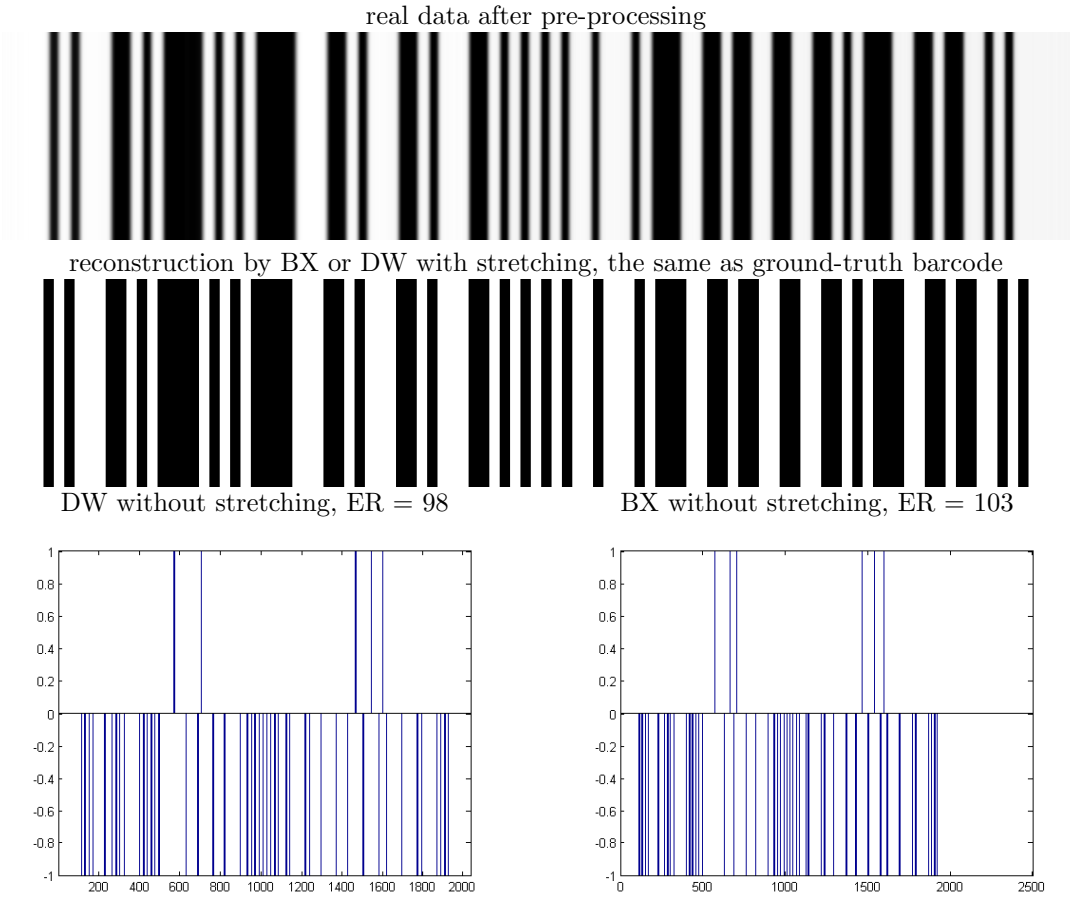

FIG. 4.6. *Deblurring results of a real image of Huggies diaper barcode. The real data is shown on the top. The reconstructions by BX or DW with stretching matrix coincide with the ground-truth barcode. Without this matrix, errors exist for both methods. The difference to the ground-truth is plotted on the last row. The errors are measured in terms of L^1 norm, which is also the number of incorrect estimates.*

of H and H^T. Since it is impossible to store this matrix, we have to compute it when needed. The definition of H is given in (5.1),

$$H \circ u(y_1, y_2) = \iint \frac{1}{2\pi r^2(s_1, s_2)} \exp^{-\frac{(y_1 - c_1(s_1, s_2))^2 + (y_2 - c_2(s_1, s_2))^2}{2r^2(s_1, s_2)}} u(s_1, s_2) \mathrm{d}s_1 \mathrm{d}s_2 \ . \quad (5.2)$$

with integration over s_1, s_2. Its transpose is expressed as

$$H^T \circ u(s_1, s_2) = \iint \frac{1}{2\pi r^2(s_1, s_2)} \exp^{-\frac{(y_1 - c_1(s_1, s_2))^2 + (y_2 - c_2(s_1, s_2))^2}{2r^2(s_1, s_2)}} u(s_1, s_2) \mathrm{d}y_1 \mathrm{d}y_2 \ . \quad (5.3)$$

with integration over y_1, y_2. Similar to 1D, we can incorporate the stretching matrix into the model. It is an up-sampling operator, while its transpose is down-sampling.

The deblurring results are presented in Figure 5.1. The synthetic blurred data shows a QR code printed on a tilted plane with the bottom left corner being further away from the camera. Neither the data nor its thresholded version can be decoded using conventional software, Zxing[3]. With the

[3]ZXing is an open-source, multi-format 1D/2D barcode image processing library implemented in Java. `https:`

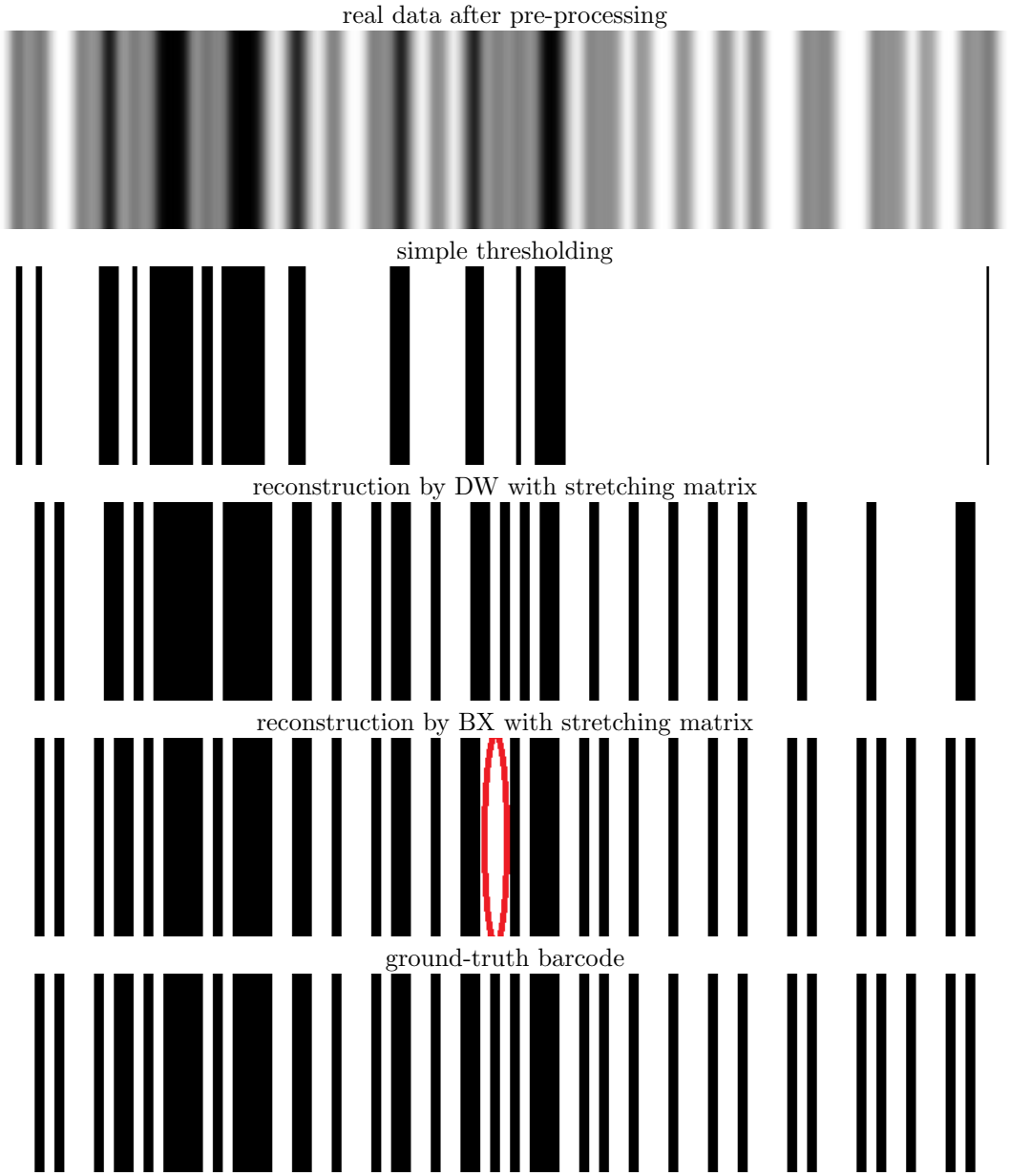

FIG. 4.7. *Deblurring results of a real image of Kirkland plastic wrap barcode. From top to bottom: real data, simple thresholding, reconstructions by BX and DW with stretching matrix and the ground-truth barcode. The real data is very blurred. The reconstruction of BX with stretching matrix is incorrect for only one bar.*

stretching matrix, either BX or DW can yield perfect reconstructions. DW without this matrix is far from being satisfactory, as it fails to preserve the corner. It might be overcome using a fourth-order PDE in [17] or wavelet double-well [10] for a general binary deblurring problem.

As for computational time, it takes 10 minutes to estimate the PSF using the LM method for a 99×99 image on Matlab. For deblurring, it takes 10 minutes for BX without stretching matrix, and 23 seconds with stretching matrix of a factor of 3. The codes run on a desktop with Intel Quad CPU 2.66Hz, 8GB RAM, Windows 7/Matlab 2009.

`//code.google.com/p/zxing/`

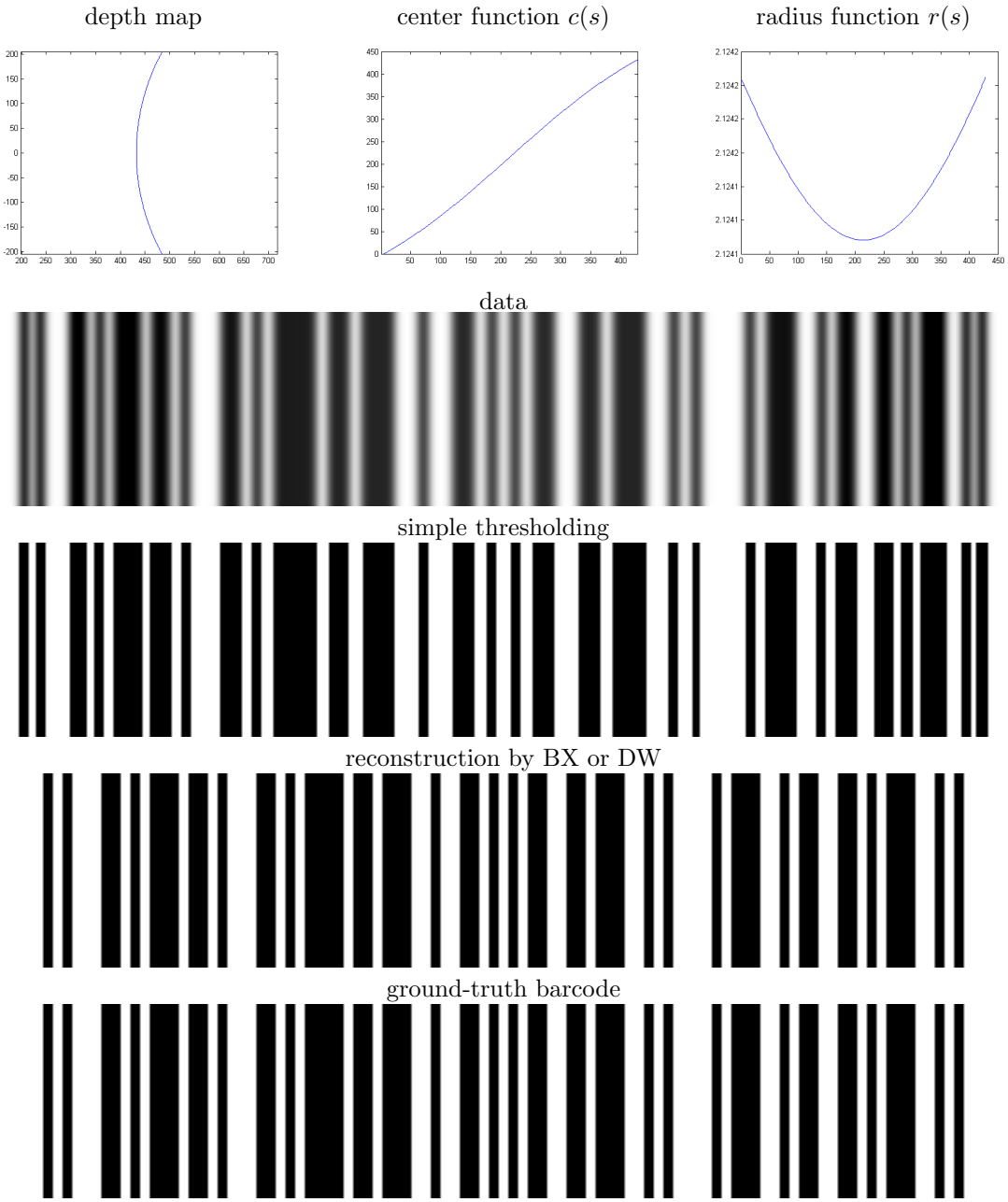

FIG. 4.8. *Deblurring results of a synthetic barcode image on a cylinder. On the first row is the depthmap, the center function $c(s)$ and radius function $r(s)$. The rest of the row are real data, simple thresholding, reconstructions by BX or DW with stretching matrix and the ground-truth barcode.*

6. Conclusions and future work. We proposed a partially blind restoration method by taking advantages of the barcode known information. In particular, a low-dimensional representation of the PSF is computed via Levenberg-Marquardt from the data and known barcode information. The image deblurring was then performed by simple quadratic programming subject to the box constraint. We find the box constraint is often a good relaxation to the binary constraint. Furthermore, we incorporated a stretching matrix into the model, which results in a significant amount of dimension reduction. It is an up-sampling operator with a factor corresponding to the minimum bar width. With the help of

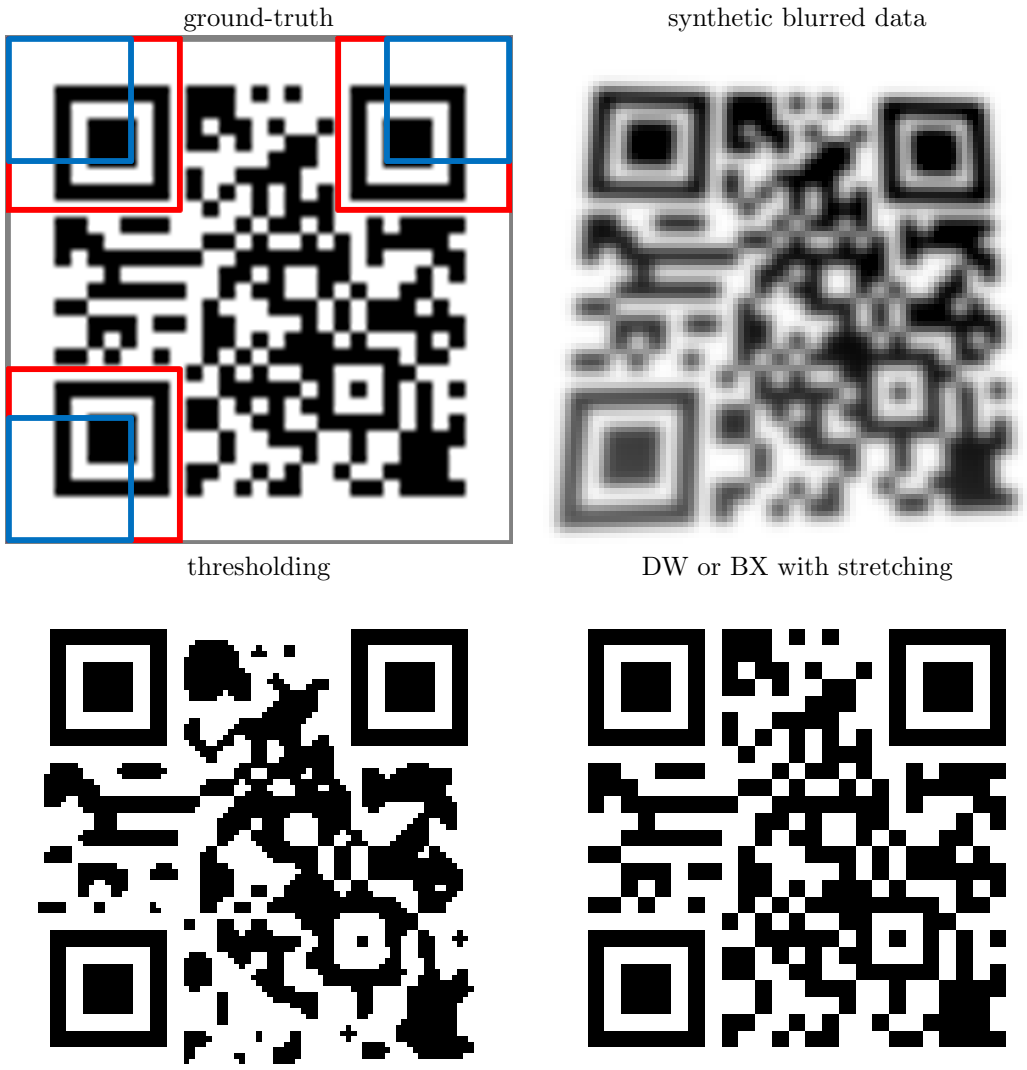

FIG. 5.1. *Deblurring of a synthetic QR code. A typical QR code is depicted on the top left. The red regions are known, and the blue regions are used to estimate the PSF. The synthetic data is shown on the top right with more blurred on the bottom left corner. With the stretching matrix, both BX and DW can get the perfect reconstruction.*

this matrix, box constraint can always give reasonable results even errors occur in estimating the PSF.

In the future, we want to study the theoretical analysis of the box constraint. For a general matrix, under what conditions can the box constraint give the same solution as the binary constraint? For barcodes, the absolute pixel values are not important, and are often sensitive to nuisance factors. It is worth searching for other quantities, such as momentum or gradient, to replace intensities as the input for the deblurring algorithm. We also want to extend this work for binary text deblurring, probably with the help of training data.

Acknowledgments - This work is supported by ONR grant N00014-11-1-0602, NSF grants DMS-0911277, DMS-0928427, and DMS-1222507.

Appendix. In this section we will derive the formula of $c(s)$ and $r(s)$for the light source coming from a general object. As depicted in Figure 2.1, we assume the origin is located at the center of the lens, the image place is placed at $x = -\nu$ and the depth map of an object be parameterized by its arc

length parameter $s \mapsto (\gamma_1(s), \gamma_2(s))$.

The light source emitted from $(\gamma_1(s), \gamma_2(s))$ goes through the center of the lens and shades a disk on the image plane. The center of this disk is the intersection of $x = -\nu$ and the line passing through the origin and $(\gamma_1(s), \gamma_2(s))$. Therefore, we have $c(s) = -\nu\frac{\gamma_2(s)}{\gamma_1(s)}$.

It follows from *thin lens formula* [19] that any light source at distance $\gamma_1(s)$ to the lens will focus on a plane with distance ν_s to the lens, which satisfies

$$\frac{1}{\gamma_1(s)} + \frac{1}{\nu_s} = \frac{1}{F} ,$$

with F being the focal length of the camera. If $\nu \neq \nu_s$, then the image of this point depends on the boundary of the lens. Assuming a thin circular lens, a point of light produces a disk, whose radius can be computed by simple similarity of triangles. The ratio between the radius of the disk and the radius of the lens is equal to $(\nu - \nu_s)/\nu_s$. Therefore, we have the radius function to be

$$r(s) = \frac{D}{2}\Big|1 - \nu(\frac{1}{F} - \frac{1}{\gamma_1(s)})\Big|$$

For barcode, it is often printed on a planar surface and thus its depth map is expressed as $x = ay+b$, whose arc length representation is

$$\begin{cases} \gamma_1(s) = s\sin\theta + b \\ \gamma_2(s) = s\cos\theta \end{cases} \tag{6.1}$$

for $a = \tan\theta$. Then we have

$$\begin{aligned} c(s) &= -\nu\tfrac{s\cos\theta}{s\sin\theta+b} = \tfrac{-\nu s}{as+b\sqrt{a^2+1}} \\ r(s) &= \tfrac{D}{2}|1 - \nu(\tfrac{1}{F} - \tfrac{\sqrt{a^2+1}}{as+b\sqrt{a^2+1}})| \end{aligned} \tag{6.2}$$

If the plane is parallel to the lens, *i.e.* $a = 0$, then the center map $c(s) = s$ after scaling. The image formation model (2.1) becomes the conventional shift-invariant blur.

REFERENCES

[1] M. Born and E. Wolf, *Principles of Optics: Electromagnetic Theory of Propagation, Interference and Diffraction of Light (7th ed.)*, Cambridge: Cambridge University Press., 1999.

[2] A. M. Bronstein, A. M. Bronstein, M. Zibulevsky, and Y. Y. Zeevi, *Blind deconvolution of images using optimal sparse representations*, IEEE Transactions on Image Processing, 14 (2005), pp. 726–736.

[3] A. M. Bruckstein, M. Elad, and M. Zibulevsky, *On the uniqueness of nonnegative sparse solutions to underdetermined systems of equations*, Information Theory, IEEE Transactions on, 54 (2008), pp. 4813 –4820.

[4] A. Chambolle and T. Pock, *A first-order primal-dual algorithm for convex problems with applications to imaging*, Journal of Mathematical Imaging and Vision, 40 (2011).

[5] S. H. Chan and T. Q. Nguyen, *Single image spatially variant out-of-focus blur removal*, in IEEE International Conference on Image Processing (ICIP), 2011, pp. 677–680.

[6] T. F. Chan, S. Esedoglu, and M. Nikolova, *Algorithms for finding glboal minimizers of image segmentation and denoising models*, SIAM J. Appl. Math., 66 (2006), pp. 1632–1648.

[7] T. F. Chan and C. K. Wong, *Total variation blind deconvolution*, IEEE Transactions on Image Processing, 7 (1998), pp. 370 – 375.

[8] S. Cho, Y. Matsushita, and S. Lee, *Removing non-uniform motion blur from images*, in IEEE International Conference on Computer Vision (ICCV), Oct. 2007, pp. 1–8.

[9] R. Choksi and Y. van Gennip, *Deblurring of one dimensional bar codes via total variation energy minimization*, SIAM J. Img. Sci., 3 (2010), pp. 735–764.

[10] J. Dobrosotskaya and A. L. Bertozzi, *Analysis of the wavelet Ginzburg-Landau energy in image applications with edges*, SIAM J. Imaging Sciences, 6 (2013), pp. 698–729.

[11] D. L. Donoho and M. Elad, *Optimally sparse representation in general (non-orthogonal) dictionaries via l1 minimization*, in Proc. Natl Acad. Sci. USA, vol. 100, 2003, pp. 2197–2202.

[12] S. Esedoglu, *Blind deconvolution of bar code signals*, Inverse Problems, 20 (2004), pp. 121–135.

[13] E. Esser, X. Zhang, and T. F. Chan, *A general framework for a class of first order primal-dual algorithms for convex optimization in imaging science*, SIAM J. Imag. Sci., 3 (2010), pp. 1015–1046.

[14] P. Favaro and S. Soatto, *A geometric approach to shape from defocus*, IEEE Transactions on Pattern Analysis and Machine Intelligence, 27 (2005), pp. 406–417.
[15] ———, *3-D Shape Estimation and Image Restoration: Exploiting Defocus and Motion Blur*, Springer Verlag, December 2006.
[16] P. Favaro, S. Soatto, M. Burger, and S. Osher, *Shape from defocus via diffusion*, IEEE Transactions on Pattern Analysis and Machine Intelligence, (2007).
[17] W. Gao and A. L. Bertozzi, *Level set based multispectral segmentation with corners*, SIAM J. Imag. Sci., 4 (2011), pp. 597–617.
[18] B. He and X. Yuan, *Convergence analysis of primal-dual algorithms for a saddle-point problem: From contraction perspective*, SIAM J. Imaging Sciences, 5 (2012), pp. 119–149.
[19] E. Hecht, *Optics (4th ed.)*, Addison Wesley, 2002.
[20] M. A. Iwen, F. Santosa, and R. Ward, *A symbol-based algorithm for decoding bar codes*, SIAM J. Imaging Sci., 6 (2013), p. 56C77.
[21] J. Jia, *Single image motion deblurring using transparency*, in IEEE Conference on Computer Vision and Pattern Recognition (CVPR), 2007.
[22] E. Joseph and T. Pavlidis, *Bar code wave-form recognition using peak locations*, IEEE Trans. Pattern Anal. Machine Intelligence, 16 (1994), pp. 630–640.
[23] S. Kresic Juric, *Edge detection in bar code signals corrupted by integrated time-varying speckle*, Pattern Recognition, 38 (2005), pp. 2483–2493.
[24] D. Krishnan, T. Tay, and R. Fergus, *Blind deconvolution using a normalized sparsity measure*, in CVPR, 2011.
[25] R. L. Lagendijk and J. Biemond, *Basic methods for image restoration and identification*, in Hand Book of image and Vedio Processing, Alan C. Bovik, ed., Academic Press, 2000, pp. 125–140.
[26] Y. Mao, *Reconstruction of binary functions and shapes from incomplete frequency information*, IEEE Trans. on Information Theory, 58 (2012), pp. 3642–3653.
[27] M.E. Moghaddam, *A mathematical model to estimate out of focus blur*, in International Symposium on Image and Signal Processing and Analysis (ISPA), 2007, pp. 278–281.
[28] J. G. Nagy and D. P. O'leary, *Restoring images degraded by spatially variant blur*, SIAM J. Sci. Comput., 19 (1998), pp. 1063–1082.
[29] M. I. Sezan, G. Pavlovic, A. M. Tekalp, and A. T. Erdem, *On modeling the focus blur in image restoration*, in Acoustics, Speech, and Signal Processing, International Conference on, vol. 4, 1991, pp. 2485 – 2488.
[30] M. Zhu and T.F. Chan, *An efficient primal-dual hybrid gradient algorithm for total variation image restoration*, tech. report, 2008. UCLA CAM Report [08-34].